Materials Science and Engineering A 615 (2014) 340--347

Effect of tempering upon the tensile properties of a nanostructured bainitic steel

H.S. Hasan[a], M.J. Peet[b,*], M-N. Avettand-Fènoël[c], H.K.D.H. Bhadeshia[b]

[a] *University of Technology, Baghdad, Iraq*
[b] *Department of Materials Science and Metallurgy, 27 Charles Babbage Road, Cambridge, CB3 0FS, UK*
[c] *Unité Matériaux Et Transformations (UMET) UMR CNRS 8207, Université; Lille 1, 59655 VILLENEUVE D'ASCQ, FRANCE*

Abstract

The tensile properties of a nanostructured carbide–free bainitic steel formed at 200–250°C are compared against those after tempering sufficiently to remove the retained austenite. Although significant ductility is observed following tempering, a comparison of tempered and untempered samples shows that it is in fact reduced when a comparison is made at identical strength. The shape of the stress-strain curves shows clear evidence that the capacity for work hardening is reduced with the loss of austenite. The nanostructure of the steel transformed at 250°C is examined by transmission electron microscopy, to compare the as–transformed to the tempered structure. In this case after tempering at 500°C the energy absorbed during the tensile test is lower, due to the lower strength. Reduction of strength is caused by the slight coarsening of the bainite plates, and lower dislocation density after tempering. Considering the formation of carbide particles in high strength steel, impressive ductility is exhibited even in the tempered condition.

Keywords: tempering, tensile properties, nanostructured steel, carbide–free bainite, transformation induced plasticity.

1. Introduction

Strong steels with a nanostructure of bainitic ferrite and austenite can be manufactured by isothermal transformation from austenite at temperatures around 200–250°C [1]. In these steels the strengthening due to the small size of the bainite plates dominates other mechanisms [1, 2]. The transformation by shear [3] at temperatures around 200°C takes more than one week to reach an asymptotic limiting fraction, or hours at higher temperatures. Careful alloy design is the only demonstrated method that can be used to accelerate the transformation while retaining the fine structure [4, 5].

In the earliest work on these steels it was observed that the hardness is relatively insensitive to quite severe tempering [1], when compared to martensitic steels of similar composition. This is because the latter derive most of

*Corresponding author
Email address: mjp54@cam.ac.uk (M.J. Peet)

their strength from interstitial carbon, which on precipitation leads to a large decrease in hardness. In the case of nanostructured bainite, intense precipitation of carbides due to the decomposition of carbon-enriched retained austenite occurs at lath boundaries – preventing the ferrite from coarsening and thus preserving the hardness and strength [6].

The fact that the austenite can decompose on tempering might be a cause for concern if the steel is to be used at elevated temperatures. Early work demonstrated that when carbide-free *microstructures* of bainitic ferrite and carbon-enriched austenite are tempered, the decomposition of the austenite, and associated carbide precipitation, leads to a decrease in toughness [7, 8]. The general philosophy is that the austenite helps improve ductility via the classical TRIP effect, in which the plasticity associated with martensitic transformation helps delay the onset of plastic instabilities during tensile testing [9–11]. The motivation for the present work was, therefore, to study the effect of severe tempering on the tensile properties of nanostructured bainite.

2. Methodology

After homogenisation for 48 h at 1200°C, steel of composition

Fe-0.78C-2.02Mn-1.01Cr-1.6Si-1.37Al-3.83Co-0.25Mo wt%

was transformed at a range of temperatures under vacuum in the Thermecmastor-Z thermomechanical simulator, with which cylindrical samples of 8 mm diameter and 12 mm in length can be induction heated under vacuum, and then rapidly cooled using inert gas. The temperature is controlled by feedback from an R-type thermocouple, and dimensional changes due to thermal expansion and solid state phase transformations can be monitored using a laser dilatometer. A portion of the samples were subjected after transformation to tempering heat treatments in a small tube furnace, and the resultant changes characterised using hardness testing, microscopy and X-ray diffraction. Vickers hardness tests are reported as the average of at least five indentations conducted using a 30 kg load.

Tensile samples with gauge length of 60 mm length and 5 mm diameter cylindrical cross section were transformed after austenitisation at 950°C for 30 minutes at 200°C for 3 days, 220°C for 3 days and 250°C for 16 h. For direct comparison half of these samples were subjected additionally to tempering at 500°C for 24 h. X-ray results (presented later) confirmed that this is sufficient to decompose all retained austenite in the steel. Transformation of the machined tensile samples was achieved by austenitisation at 950°C in a tube furnace purged with a positive pressure of argon gas, before manual transfer to an oven with temperature stability better than 0.1°C for isothermal transformation at the various temperatures.

Tensile tests were conducted at room temperature using an Instron 2527-111 machine with a crosshead speed of 0.1 mm min^{-1}. A strain gauge was attached to the gauge length with an initial distance between the strain gauge knife edges of 25 mm. The area under the stress–strain curve was integrated to assess the work of fracture.

Fracture surfaces were examined using scanning electron microscopy (Camscan MX2600 FEGSEM), and inspection of the cross section of the sample

perpendicular to the fracture surface was made using a JEOL 6340 FEGSEM operated at 15 kV.

X-ray diffraction experiments were conducted using a Philips PW1830 counter diffractometer with Cu K_α radiation, at a scan rate of $0.03\,^\circ\,\mathrm{min}^{-1}$ over the range $35 \leq 2\theta \leq 105^\circ$ and the system operating at 40 kV and 40 mA. Rietveld analysis was applied to fit the whole diffraction pattern using Philips X'Pert HighScore plus software, to determine austenite and ferrite phase fractions.

Transmission electron microscopy (TEM) with an accelerating voltage of 200 kV was also performed on thin foils for the specimen homogenised at 1200°C for 2 days, austenised at 950°C for 30 min under argon and isothermally held at 250°C for 16 h. Thin foils were ground to 50 μm and finally electrochemically thinned using a Struers Electropol twin jet polishing system to produce an electron transparent volume. The electrolyte was composed in volume of 5% perchloric acid, 15% glycerol and 80% of methanol. Polishing occurred with a potential of 32 V at -34°C and a current density of 5.7 $\mathrm{A\,mm}^{-2}$ for the as–transformed bainitic structures. For the specimens tempered at 500°C for 1 day the conditions were 22.5 V, -17.7°C.

3. Results

Figure 1 shows the change in hardness with tempering time for samples transformed at different transformation temperatures (200, 220 and 250°C) and then tempered at 500°C for different times. Based on previous experience, tempering for 24 h was estimated to be sufficient to ensure that retained austenite had decomposed fully [6, 12–14]. X-ray diffraction was used to investigate the austenite fraction after tempering, finding none present. As seen in the figure, most of the hardness decrease had occurred by 24 h.

There is a marked change in tensile behaviour as a consequence of the tempering (Figure 2 and Table 1). Rather than the classical shape of parabolic hardening following gradual yielding, linear hardening at a lower rate is observed after a distinct yield point until fracture. At the same time the elongation observed is higher in comparison to the as–transformed condition in each case. This behaviour was observed regardless of the transformation temperature used. The tensile results for the samples transformed at 250°C are notable, in that samples before and after tempering both have around 10% elongation. Toughness as measured by the area under the stress–strain curve is reduced, due to the lower tensile strength.

In the as-transformed state the hardness is observed to increase with decreasing transformation temperature, while the elongation decreases. Upon tempering the hardness values began to converge. Despite this, the tensile properties still had a strong dependence upon the isothermal transformation temperature.

X-ray diffraction patterns were collected from samples before and after tempering at 500°C for 1 day (Figure 3). They show, as expected from the increase in driving force as a function of undercooling, that the volume fraction of austenite in the as-transformed samples decreased as the isothermal transformation temperature was reduced and show that the tempering reduced the retained austenite to negligible amounts in all cases (Table 2). No austenite peaks could be distinguished after tempering, considering the isolated austenite (220) peak the lowest fraction of austenite detectable at the 99% confidence level is calculated to be 0.04% assuming a peak width of 2 degree 2θ.

The larger quantity of austenite associated with the 250°C sample is consistent with its greater ductility in the as-transformed condition. The higher carbon supersaturation of the austenite in this sample is unexpected on the basis of thermodynamic criteria alone; although a similar trend has been observed previously [1, 15, 16]. It is clear from Table 2 that $V_\gamma x_\gamma + (1 - V_\gamma)x_\alpha \neq \overline{x}$, where $\overline{x}$ is the average concentration of carbon in the steel, i.e. 0.79 wt%.

These issues can be resolved with the knowledge, consistent with atom-probe observations, that carbon is not just present in solid solution in the bainitic ferrite [17, 18] but also located at defects such as dislocations. Such trapped carbon is located at positions where the lattice is already dilated due to the strain field of the defect [19]. We assume that the expansion of the lattice parameter as detected by measuring the lattice parameter using X-ray diffraction, does not account for heterogeneous strains due to defects since such defects lead to peak broadening, but is largely due to carbon in solid solution. It follows that the residue $x_\rho = \overline{x} - V_\gamma x_\gamma - (1 - V_\gamma)x_\alpha$ is the trapped carbon, then the data indicate that the defect density must increase as the transformation temperature is reduced. This, of course, is exactly as expected since both the dislocation density and the amount of interfacial area per unit volume increase as the bainite is produced at a lower temperature [20]. Notice that carbon is known to be trapped in defects within both ferrite and austenite, so the values of x_ρ in Table 2 are not particularly large. This hypothesis would also explain the larger x_γ of the sample transformed at 250°C, because less carbon is trapped in the defects in its coarser and softer structure, making more available for partitioning into the austenite. The concept described here, and the concentrations involved, are consistent with early work [21] that demonstrated quantitatively that high concentrations of carbon (< 0.45 wt%) can be associated with dislocation densities typical of lath martensite; the new aspect here is to claim that the segregation of carbon to such defects does not lead to significant lattice expansion.

Figure 4 shows the fractographs for the as-transformed samples at different transformation temperatures (220, 250°C) and also after subsequent tempering for 1 day at 500°C. The fracture surfaces of the untempered samples consist of many microvoids and dimples, with a small amount of intergranular separation at the austenite grain boundaries. The major mechanism of ultimate failure in the untempered sample is by ductile nucleation and growth of voids, and the final shearing of the specimen produces a cup and cone fracture as seen from Figure 5.

As previously observed, and shown in the transmission electron microscopy presented later, a fine dispersion of carbides results from the decomposition of retained austenite completely into a mixture of ferrite and carbides during tempering. In the tempered samples the dimples observed on the fracture surface are much finer, consistent with the presence of many carbides from which void nucleation can occur. Crack propagation along the grain boundaries is more prevalent and the major mechanism of ultimate failure is by quasi-cleavage. In quasi-cleavage, cleavage occurs on a very fine scale between the array of carbide particles. A fine network of cracks initiates and as the stress increases the cleavage extends by tearing into the ferrite matrix around it by microvoid coalescence. This failure mechanism has sufficient toughness to allow the tempered sample to possess a higher elongation than the as–transformed condition as seen in Figure 2. Figure 6 shows the microstructure for the area within 200 μm of the fracture surface of the as transformed sample at 250°C and the tempered

sample at 500°C for 1 day. The plasticity before failure is demonstrated by the existence of voids just below the fracture surface, and the observation of necking at the macroscopic scale.

Figure 7 shows the structure of the untempered specimen homogeneised at 1200°C for 2 days, austenised at 950°C for 30 min under argon and isothermally held at 250°C for 16 h. The selected area electron diffraction pattern proves the existence of bainitic ferrite crystals (two orientations), together with austenite that is intercalated between the ferrite platelets (Figure 7). The thin plates of bainitic ferrite are highlighted in figure 7c, which shows an example dark field image taken using the spot indexed as $[\bar{1}01]_\alpha$ in Figure 7c.

The influence of tempering is illustrated in Figure 8 with some indications of bainitic ferrite plate coarsening, as established quantitatively. The mean linear intercept ($\overline{L}_T^\alpha$) measured normal to the projected long directions of thin plates is related to their true thickness as follows [22, 23]:

$$\overline{L}_T^\alpha = \pi t/2 \qquad \text{with the 95\% confidence error} \qquad E = \pm 2\sigma_L^\alpha/(\pi\sqrt{N}) \qquad (1)$$

where σ_L^α standard deviation of the intercepts, N the number of measurements.

For the specimen isothermally held at 250°C for 16 h, the true thickness of the plates is close to 38±3 nm whereas the value is found to be 43±4 nm for the sample tempered at 500°C for 1 day. These values are similar within the confidence limits, consistent with previous work [12] that indicated the remarkable resistance of the nanostructure to coarsening.

A comparison of Figures 8a and 8b further shows that instead of austenite at the interface of the bainitic ferrite plates, some fine carbides have precipitated during tempering at 500°C for 1 day. Accounting for stereology [24, 25] from the analysis of 182 precipitates, the volume fraction and the interspacing of precipitates were estimated as 2.47% and 60 nm, respectively with a mean radius of 5.8 nm. These calculations were performed assuming that precipitates are are equiaxed and that the thin foil had a thickness of 50 nm.

4. Discussion

In order to better understand the change in mechanical properties upon tempering, calculations were performed to evaluate the strength contributions to the bainitic ferrite in the material transformed at 250°C in the as-transformed and tempered condition. The strength in MPa has been expressed in previous work by equation 2 [26, 27] for 0.4C wt% alloys. Although this formulation is not directly applicable to the total strength in this case, especially as it neglects composite effects due to a microstructure containing retained austenite, it provides a useful indication of the magnitude of the various strength contributions.

$$\sigma = \sigma_{Fe} + \sum_i \sigma_{SS,i} + \sigma_C + \frac{115}{\overline{L}_T^\alpha} + 7.34 \times 10^{-6}\sqrt{\rho_D} + \frac{42}{\lambda_p} \qquad \text{MPa} \qquad (2)$$

where σ_{Fe} is the strength of pure annealed iron, $\sigma_{SS,i}$ the solid solution strengthening due to substitutional solute i and σ_C the solid solution due to carbon. $\sigma_{SS,i}$ = 84.%Si + 32.%Mn + 13.%Mo - 30.%Cr [28, 29], $\sigma_C = 1722.5\sqrt{\%\text{C}}$ where the alloying elements are all in solution in the bainitic ferrite [26]; the

concentrations are in wt%. $\overline{L}_T^{\alpha}$ is the mean lineal intercept of bainitic ferrite plates expressed in μm, ρ_D the dislocation density in m^{-2}, and λ_p the distance between carbide particles on the slip plane in μm.

Smith and Hehemann [30] studied hardening by cementite precipitation in 0.4C-1.8Ni-Cr-Mo wt% carbon martensitic steel (AISI 4340). They expressed the particle strengthening (σ_p in MPa) in terms of the average distance between two particles on the slip plane (λ_p). Assuming a cubic distribution they provided the formulation;

$$\sigma_p = \frac{42}{\lambda_p} = \frac{42}{r\left(\left(\frac{2\pi}{3f}\right)^{1/2}\right) - \frac{\pi}{2}} \qquad \text{MPa} \tag{3}$$

where r is the radius and f is the volume fraction of precipitates.

Calculation of the interparticle spacing on the slip plane is necessary for the formulation applied to particle strengthening; this is different to the true particle spacing which can be calculated following Frommeyer [25], also from the radius and volume fraction, as 60 nm.

From measurements of precipitate radius of 5.8 nm and using the thermodynamically calculated volume fraction of cementite of 0.0025, the predicted contribution due to precipitate strengthening is 265 MPa.

Table 3 summarises the individual strengthening contributions for the specimen in two conditions: isothermally held at 250°C for 16 h, and also subsequently tempered at 500°C for 1 day. The purpose is to illustrate the relative magnitudes of the individual contributions to yield strength, rather than to calculate the actual strength in a tensile test. On tempering the small increase in the bainite plate size leads to a proportional decrease in the strength contribution. Strength contribution due to other factors is greatly reduced, and partially compensated for by the addition of precipitate strengthening.

It is noticeable that the strength of the as-transformed material is greatly overestimated, assuming that the individual contributions can simply be summed. In reality, similar analyses indicate a power-weighted sum, $\sigma^k = \sum {\sigma_i}^k$, where k is essentially a fitting constant [31, 32, e.g.]. If, for example, we choose $k \approx 3$, then the strength levels predicted are close to those observed, but the choice of k is empirical so this approach is not generally recommended at this time.

Secondly, the calculation neglects the presence of austenite; nanoindentation experiments on nanostructured bainite similar to the present work, and following transformation at 250°C, have demonstrated that the austenite is much weaker [33]. Indeed, the ratio of the hardness of austenite to ferrite was found to be 0.69 [33]. Composite theory [34, 35] indicates that because of a stress focusing effect, deformation in such a mixed structure will begin at a stress *less than* 0.69 of the calculated strength of the ferrite, i.e. $< 0.69 \times 3249 = 2256$ MPa. Furthermore, as deformation progresses, the TRIP effect continues to provide a hardening mechanism until the austenite content loses percolation resulting in fracture [11]. There is nevertheless, a need for further understanding of the deformation behaviour of such fine structures containing plate-like grains, because it is not clear whether the terms listed in Table 3 are strictly additive. For example, the strong solid-solution contribution from carbon may override any smaller barriers due to dislocation forests.

Transformation at 250°C resulted in a fraction of 0.21 retained austenite, as a result of ductile fracture around 0.1 fraction is expected to remain after the

tensile test. As noted in the results section, the difference in strain hardening with and without austenite present results in higher total energy absorbed ($87 - 75 = 12\,\mathrm{MJ\,m^{-3}}$ or $86\ \mathrm{J\,mol^{-1}}$). This value is equivalent to the transforming austenite absorbing an energy of $782\ \mathrm{J\,mol^{-1}}$, a value similar to the stored energy resulting from martensite transformation (usually around 700–1200 $\mathrm{J\,mol^{-1}}$).

A key difference also is that the strain hardening capacity in the untempered samples is clearly greater than after tempering, consistent with the role of retained austenite via the TRIP effect. As a consequence, the combinations of properties after tempering are not improved in comparison to as–transformed nanostructures of the same strength level as demonstrated in Figure 9.

5. Conclusions

The present work shows that tempering of hard–nanostructured–bainitic steels to remove austenite can result in steels which maintain or have improved elongation in spite of an intense precipitation of carbides at the plate boundaries. This comes at the cost of lowering the strength of the steel, just as occurs classically in the tempering of quenched martensitic steels.

After tempering the strength contribution from the scale of the bainite plates becomes increasingly dominant. Quite severe tempering leads to a removal of carbon that has remained in solid solution in the bainitic ferrite, and a recovery of the structure without significant coarsening of the plates. The contribution to the strength made by the carbide particles is relatively small.

Comparison of the stress–strain curve of as–transformed and tempered nanostructure vividly illustrates the benefit of retained austenite in achieving additional strain hardening, with strain hardening resulting from the additional energy needed to transform austenite to martensite during deformation.

The observation bodes well for the design of nanostructured steel for use at elevated temperatures. Whilst the retention of austenite has been demonstrated to be beneficial, useful mechanical properties are still possible even upon tempering.

6. Acknowledgements

The authors would like to thank Professor A. L. Greer for the provision of laboratory facilities at the University of Cambridge and also express their gratitude to the Scholars Rescue Fund of International Institute of Education in Washington DC, for supporting Hala Salman Hasan's work in Cambridge. We also thank Dr. Yan Pei and Dr. Lucy Fielding for helpful discussion.

References

[1] F. G. Caballero, H. K. D. H. Bhadeshia, K. J. A. Mawella, D. G. Jones, and P. Brown. Very strong, low–temperature bainite. *Materials Science and Technology*, 18:279–284, 2002.

[2] C. G. Mateo and F. G. Caballero. Ultrahigh–strength bainitic steels. *ISIJ International*, 45:1736–1740, 2005.

[3] M. Peet and H. K. D. H. Bhadeshia. Surface relief due to bainite transformation at 473 K. *Metallurgical & Materials Transactions A*, 42:3344–3348, 2011.

[4] C. Garcia-Mateo, F. G. Caballero, and H. K. D. H. Bhadeshia. Acceleration of low–temperature bainite. *ISIJ International*, 43:1821–1825, 2003.

[5] H. S. Hasan, M. Peet, H. K. D. H. Bhadeshia, S. Wood, and E. Watson. Temperature cycling and the rate of the bainite transformation. *Materials Science and Technology*, 26:453–456, 2010.

[6] M. Peet. *Transformation and tempering of low–temperature bainite*. PhD thesis, University of Cambridge, Cambridge, U. K., 2010.

[7] H. K. D. H. Bhadeshia and D. V. Edmonds. Bainite in silicon steels: a new composition property approach I. *Metal Science*, 17:411–419, 1983.

[8] H. K. D. H. Bhadeshia and D. V. Edmonds. Bainite in silicon steels: a new composition property approach II. *Metal Science*, 17:420–425, 1983.

[9] M. Sherif, C. Garcia-Mateo, T. Sourmail, and H. K. D. H. Bhadeshia. Stability of retained austenite in TRIP–assisted steels. *Materials Science and Technology*, 20:319–322, 2004.

[10] M. Y. Sherif. *Characterisation and development of nanostructured, ultra-high strength, and ductile bainitic steels*. University of Cambridge, 2005.

[11] H. K. D. H. Bhadeshia. Nanostructured bainite. *Proceedings of the Royal Society of London A*, 466:3–18, 2010.

[12] C. Garcia-Mateo, M. Peet, F. G. Caballero, and H. K. D. H. Bhadeshia. Tempering of a hard mixture of bainitic ferrite and austenite. *Materials Science and Technology*, 20:814–818, 2004.

[13] H. S. Hasan, M. J. Peet, and H. K. D. H. Bhadeshia. Severe tempering of bainite generated at low transformation temperatures. *International Journal of Materials Research*, 103:1319–1324, 2012.

[14] C. N. Hulme-Smith, I. Lonardelli, M. J. Peet, A. C. Dippel and H. K. D. H. Bhadeshia. Enhanced thermal stability in nanostructured bainitic steel. *Scripta Materialia*, 69:191-194, 2013.

[15] C. Garcia-Mateo, F. G. Caballero, and H. K. D. H. Bhadeshia. Low–temperature bainite. *Journal de Physique Colloque*, 112:285–288, 2003.

[16] C. Garcia-Mateo and F. G. Caballero. Role of retained austenite on tensile properties of steels with bainitic microstructures. *Materials Transactions*, 46:1839–1846, 2005.

[17] F. G. Caballero, M. K. Miller, C. Garcia-Mateo, and J. Cornide. New experimental evidence of the diffusionless transformation nature of bainite. *Journal of Alloys and Compounds*, 577:S626–S630, 2013.

[18] F. G. Caballero, M. K. Miller, C. Garcia-Mateo, J. Cornide, and M. J. Santofimia. Temperature dependence of carbon supersaturation of ferrite in bainitic steels. *Scripta Materialia*, 67:846–849, 2012.

[19] A. Seegar and P. Haasen. Density changes of crystals containing dislocations. *Philosophical Magazine*, 3:470–475, 1958.

[20] H. K. D. H. Bhadeshia. *Bainite in Steels, 2nd edition*. Institute of Materials, London, U.K., 2001.

[21] D. Kalish and M. Cohen. Structural changes and strengthening in the strain tempering of martensite. *Materials Science and Engineering*, 6:156–166, 1970.

[22] L. C. Chang and H. K. D. H. Bhadeshia. Austenite films in bainitic microstructures. *Materials Science and Technology*, pages 874–881, 1995.

[23] H.K.D.H. Bhadeshia. Introduction to quantitative metallography. Part II lecture notes, 2013.

[24] J. W. Cahn and J. Nutting. Transmission quantitative metallography. *Transations of the Metallurgical Society of AIME*, 15:526–528, 1959.

[25] G. Frommeyer. *Physical Metallurgy, eds R. W. Cahn and P. Haasen*, volume 2. Elsevier, Amsterdam, Holland, 1983.

[26] C. H. Young and H. K. D. H. Bhadeshia. Strength of mixtures of bainite and martensite. *Materials Science and Technology*, 10:209–214, 1994.

[27] J. Daigne, M. Guttmann, and J. P. Naylor. Influence of lath boundaries and carbide distribution on the yield strength of 0.4%C tempered martensitic steels. *Materials Science and Engineering*, 56:1–10, 1982.

[28] F. B. Pickering and T. Gladman. Metallurgical developments in carbon steels. Technical Report Special Report no. 81, Iron and Steel Institute, London, U.K., 1963.

[29] G. R. Speich and H. Warlimont. Yield strength and transformation substructure of low carbon martensite. *J. Iron and Steel Institute*, 206:385–392, 1968.

[30] D. W. Smith and R. F. Hehemann. Influence of structural parameters on the yield strength of tempered martensite and lower bainite. *Journal Iron and Steel Institute*, 209(6):476–481, 1971.

[31] K. L. Kendig and D. B. Miracle. Strengthening mechanisms of an Al-Mg-Sc-Zr alloy. *Acta Materialia*, 20:4165–4175, 2002.

[32] S. Schänzer and E. Nembach. The critical resolved shear stress of γ'-strengthened nickel-based superalloys with γ'-volume fractions between 0.07 and 0.47. *Acta Metall. Mater.*, 40(4):803–813, 1992.

[33] H. F. Lan, X. H. Liu, and L. X. Du. Ultra–hard bainitic steels processed through low temperature heat treatment. *Advanced Materials Research*, 156–157:1708–1712, 2011.

[34] Y. Tomota, K. Kuroki, T. Mori, and I. Tamura. Tensile deformation of two ductile phase alloys: flow curves of α/γ Fe–Cr–Ni alloys. *Materials Science and Engineering*, 24:85–94, 1976.

[35] H. K. D. H. Bhadeshia and D. V. Edmonds. Analysis of the mechanical properties and microstructure of a high–silicon dual phase steel. *Metal Science*, 14:41–49, 1980.

[36] H. Lan, L. Du, and X. Liu. Effect of austempering route on microstructural characterization of nanobainitic steel. *Acta Metallurgica Sinica (English Letters)*, 2014. DOI:10.1007/s40195-013-0006-2.

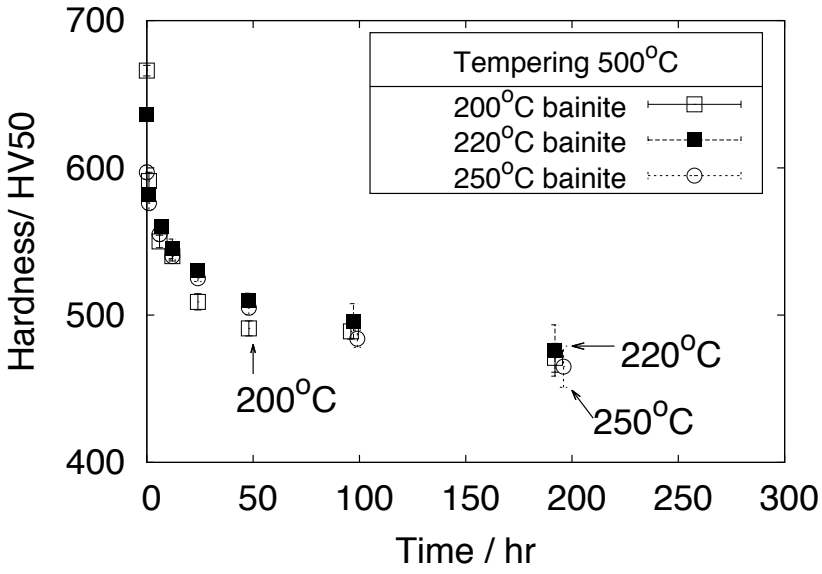

Figure 1: Hardness evolution during tempering at 500°C.

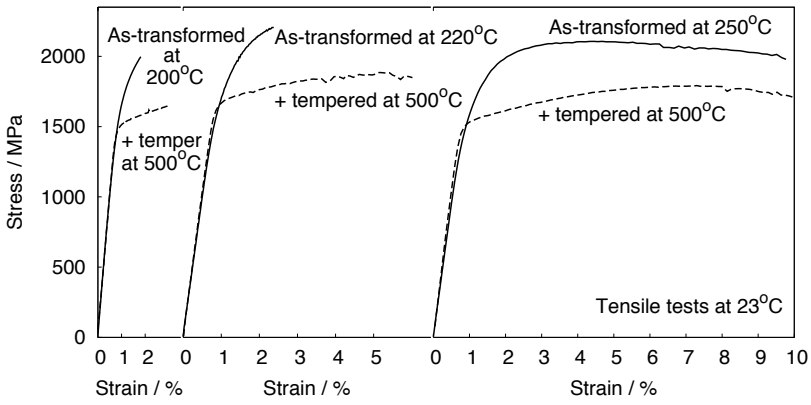

Figure 2: Stress–strain curves of steels in as–transformed (at 200, 220, 250°C) and as–tempered state (500°C for 1 day).

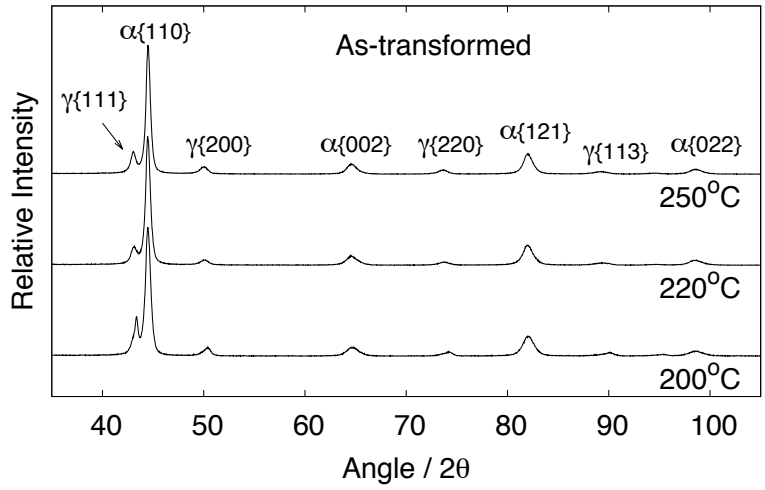

(a)

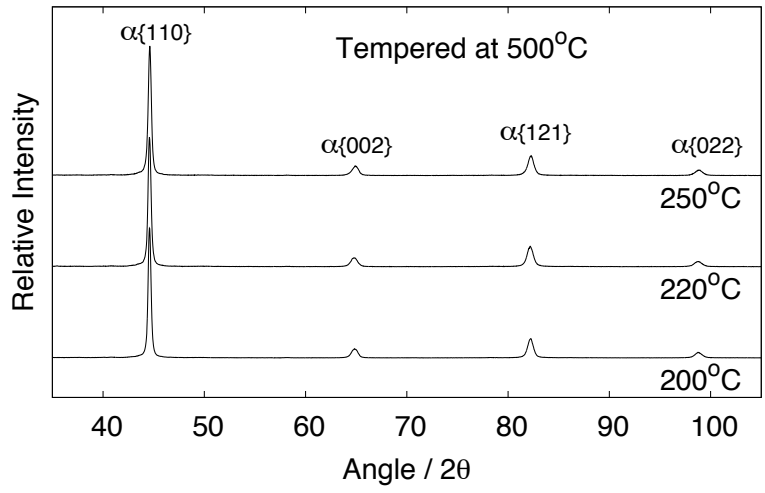

(b)

Figure 3: X-ray diffraction pattern of the alloy steel specimen transformed at different transformation temperatures (200, 220, 250°C) before (a) and after (b) tempering at 500°C for 1 day.

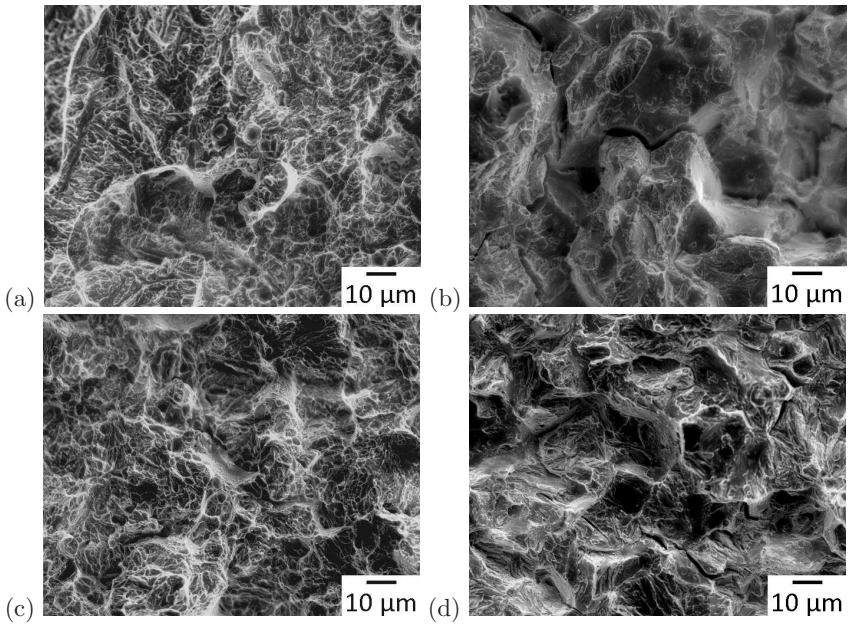

Figure 4: Scanning electron micrographs of the fracture surfaces of untempered samples at different transformation temperatures (a) 220°C, (b) 250 °C, and corresponding tempered samples (c) 220°C (d) 250°C after 500°C for 1 day.

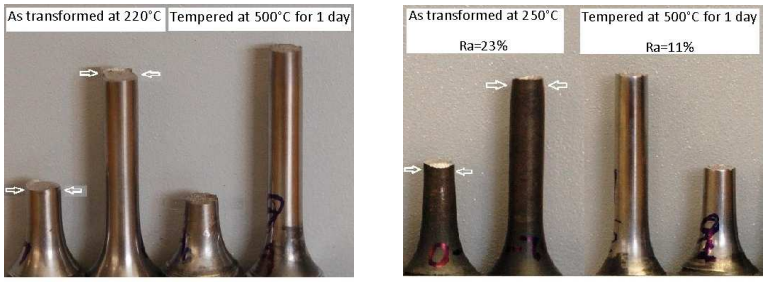

(a) (b)

Figure 5: Tensile Samples before (a) and after (b) tempering.

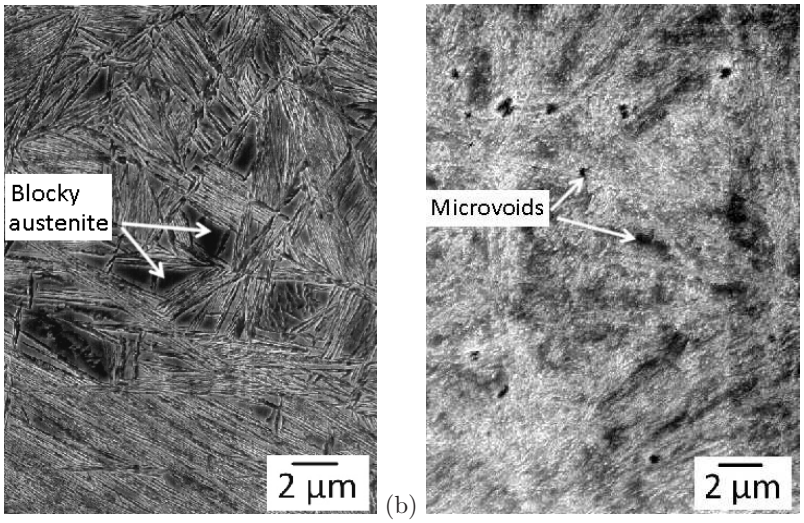

Figure 6: Scanning electron micrographs of the area below the fracture surfaces of (a) as-transformed (250°C) sample and (b) after tempering at 500°C for 1 day. Austenite blocks have been removed by tempering process and carbide precipitation has occurred, as confirmed by transmission images presented later. Microvoids evident in the tempered tensile sample could not be confidently associated with microstructural features.

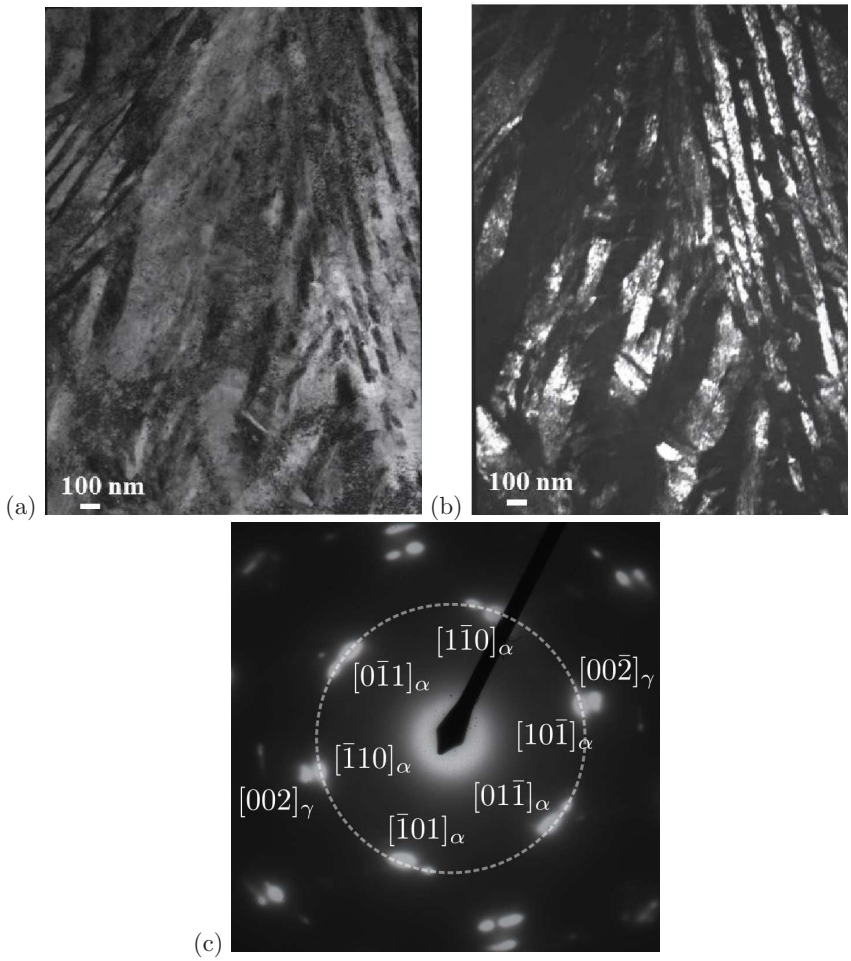

Figure 7: Structure of the specimen isothermally held at 250°C for 16 h without tempering, (a) bright field micrograph, (b) dark field micrograph corresponding to ferrite $[\bar{1}01]_\alpha$ as shown in (c) indexed electron diffraction pattern for the [111] zone axis of bainitic ferrite and the [110] zone axis of austenite.

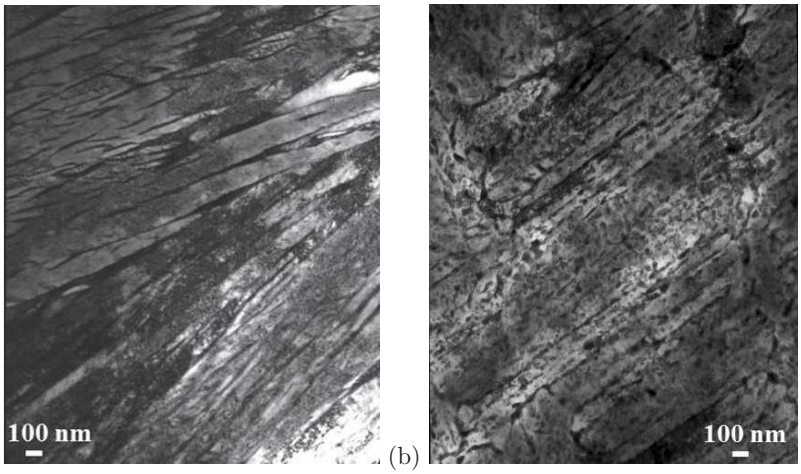

Figure 8: Structure of the specimen isothermally held at 250°C for 16 h without tempering (a) and with tempering at 500°C for 1 day (b)

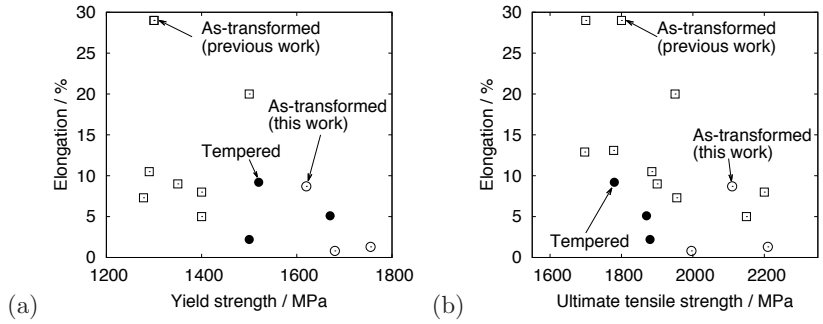

Figure 9: Strength and elongation as a result of tempering at 500°C (filled circles) compared to those of the as–transformed steels. Unfilled circles are for this work, unfilled squares represent previously reported results for as–transformed low–temperature bainite [4, 36].

Table 1: Mechanical properties observed for the as-transformed, and also after tempering at 500°C.

Transformation temperature/ °C, condition	Hardness / HV50	Yield strength strength / MPa	Tensile strength / MPa	Elongation / %	Energy absorbed / $MJ\,m^{-3}$
200	666±4	1880	1996	0.8	6.6
220	636±4	1755	2210	1.3	10.5
250	597±5	1620	2110	8.7	87.2
200, tempered	509±6	1500	1680	2.2	13.0
220, tempered	530±3	1670	1870	5.1	43.6
250, tempered	525±2	1520	1780	9.2	75.1

Table 2: Compiled results for X-ray diffraction data. a_γ and a_α represent the lattice parameters of austenite and ferrite respectively, with a Rietveld fitting error of ≤ 0.001 Å. x_γ and x_α are the respective carbon concentrations and x_ρ is estimated the concentration of carbon trapped at defects.

Transformation temperature / °C, condition	V_γ	a_γ / Å	a_α / Å	x_γ / wt%	x_α / wt%	x_ρ / wt%
200	0.17±0.01	3.6218	2.8753	1.23	0.26	0.37
220	0.18±0.01	3.6209	2.8748	1.23	0.24	0.37
250	0.21±0.01	3.6366	2.8671	1.68	0.22	0.53
200, tempered	0.000 (<0.0004)	-	2.8721	-	0.14	-
220, tempered	0.000 (<0.0004)	-	2.8706	-	0.10	-
250, tempered	0.000 (<0.0004)	-	2.8621	-	0.15	-

Table 3: Effect of tempering on the respective contributions of various factors to the strengthening of the specimen isothermally held at 250°C for 16 h. The dislocation densities of the untempered and tempered samples have been taken to be 6.3×10^{15} m^{-2} [26] and 7×10^{13} m^{-2} respectively. A 50 nm thin foil has been assumed with respect to the stereological determinations for carbides.

Structural Component	Strengthening contributions / MPa	
	As-transformed	Tempered
Fe	168	168
Solid solution of C and other solutes	986	178
Thickness of the bainitic ferrite plates	1513	1337
Dislocations	583	60
Carbides	0	265
Sum of contributions $\sigma = \sum \sigma_i$	3250	2008
Power-weighted sum $\sigma^k = \sum {\sigma_i}^k$, $k = 3.0$	1666	1324